Journal of Molecular Liquids 392 (2023) 123177

Contents lists available at ScienceDirect

Journal of Molecular Liquids

journal homepage: www.elsevier.com/locate/molliq

An investigation on spectroscopic, wavefunction dependent reactivity, docking and anti-Covid-19 ability of flupentixol dihydrochloride: DFT and MD simulations at different temperatures

Jamelah S.Al-Otaibi [a,*], Y.Sheena Mary [b], Y.Shyma Mary [c], Nivedita Acharjee [d], Deepthi S. Rajendran Nair [e], H.S. Yathirajan [f]

[a] Department of Chemistry, College of Science, Princess Nourah Bint Abdulrahman University, P.O. Box 84428, Riyadh 11671, Saudi Arabia
[b] Department of Physics, FMNC, University of Kerala, Kollam, Kerala, India
[c] Thushara, Neethinagar-64, Pattathanam, Kollam, Kerala, India
[d] Department of Chemistry, Durgapur Government College, District-Paschim Bardhaman, West Bengal, India
[e] Department of Ophthalmology, Keck School of Medicine, University of Southern California, Los Angeles, CA 90033, USA
[f] Department of Studies in Chemistry, University of Mysore, Manasagangotri, Mysore, Karanataka, India

ARTICLE INFO

Keywords:
Flupentixol
DFT
AIM analysis
MD simulations
Docking

ABSTRACT

A detailed vibrational analysis of flupentixol dihydrochloride (FDC) is performed by Density Functional Theory (DFT) calculations. Wavefunction reactivity properties and Atoms In Molecules (AIM) analysis are also performed. There is enormous O_1-H_{1B}…Cl_1, N_1-H_{1A}…Cl_1 and C_9-H_{9A}…F_{3B} intermolecular hydrogen bonding in FDC. Electrons were resonated on the aromatic rings without any interference with aliphatic moiety of both highest occupied molecular orbital (HOMO) and in least unoccupied molecular orbital (LUMO) which is due to participation of fluorine atom intermolecular hydrogen bonding with adjacent C–H. The electron localization function (ELF) shows under populated N-C single bonds of ring A owing to the strong electron withdrawing effect of nitrogen atoms. SARS-CoV-2 main protease with FDC had energy −80 kcal/mol. With the help of molecular dynamics (MD), radial distribution functions (RDF) are calculated to identify the most critical interaction with water molecules.

1. Introduction

Tricyclic aromatic ketones have been used as starting materials for the production of trycyclic medicines, as well as causing overcrowding in bistricyclic enes [1]. Thioxanthene and numerous of its derivatives have been found to have biologically beneficial properties [2]. However, early clinical trials have revealed that several of the most promising therapeutic candidates derived from this family of chemical have negative hazardous characteristics [3]. In the photo polymerization of ethylene derivatives, various thioxanthone derivatives are utilized as activators or sensitizers [4]. Substituted thioxanthones are employed as radical sources as stabilizers for polyolefins [5]. This family of compounds has been used in a variety of industrial operations. Flupentixol is a thioxanthene derivative with antipsychotic characteristics that is commonly used for diseases with anxiety as a symptom [6]. Flupentixol is a medicine that is commonly administered in India due to the rise in psychiatric disorder. As a result, it is frequently detected in waste water, necessitating a good removal technique [7]. Phenothiazine and similar structures are used to treat psychotic diseases all over the world [8]. Many phenothiazine compounds have powerful antiemetic, antihistaminic or anti-cholinergic properties [9]. Several medications have been observed to interact with phenothiazine antipsychotic medicines [10,11]. They enhance the effect analgesics, anti-histaminics and cold treatments that have been prescribed. Low dose neuroleptics are increasingly being used to treat anxiety and depression [12]. Balasubramani et al., reported removal of flupentixol using graphene oxide [13]. Studies of drug interaction between levocetirizine are reported [14]. El-Zahry and Lendl reported the kinetic study of ofloxacin using SERS [15]. Raghav et al., reported interactions of trifluoperazine with serum albumin using multi spectroscopic methods [16]. Spectroscopic studies of thioxanthens are reported [17,18]. The piperazine ring plays a larger role in drug development, with a higher number of favourable hit

* Corresponding author.
E-mail address: jamelah2019@rediffmail.com (J. S.Al-Otaibi).

https://doi.org/10.1016/j.molliq.2023.123177
Received 23 April 2023; Received in revised form 27 July 2023; Accepted 24 September 2023
Available online 27 September 2023

sin biological applications and characteristics. In medicinal chemistry, it is a strong and selective ligand for a variety of biological targets. Piperazine structure and scaffolds have been identified as biologically active medicinal compounds and have been classed as favoured structures. Due to its relationship with a variety of biological and therapeutic uses, chemists have been studying piperazine derivatives extensively [19–26]. Piperazine scaffolds can found in a variety of physiologically active drugs used to treat human immunodeficiency virus (HIV), and as inhibitors of SARS-CoV-2 enzyme [27–29]. Siddegowda et al., reported X-Ray diffraction (XRD) analysis of flupentixol dihydrochloride (FDC) [30]. Jomma et al., reported the insight into non-covalent interactions in a tetrachlorocadmate salt with promising nonlinear optical properties experimentally and theoretically [31]. Issaoui et al., reported the experimental and theoretical studies on novel derivative of acrylic acid and molecular docking with temperature dependency of the thermodynamic functions [32]. Morphine's non covalent interactions and molecular docking studies are recently reported and the analysis revealed different categories on inter- and intra-molecular contacts on the basis of the electron localization density and colour scale indicator [33]. Evecen et al., reported the XRD and theoretical investigations of a methoxyphenyl-pyrazole derivative [34]. A single crystal X-ray diffraction analysis shows that a tris β-diketonate europium (III) is octacoordinated and the coordination sphere is composed of a EuO_6N_2 core with trigonal dodecahedral geometry [35]. Sen et al., reported peripherally tetra-benzimidazole units-substituted zinc (II) phthalocyanines and its photochemical properties [36]. The crystal structure and Hirshfeld surface analysis of a pyridine-benzoxa-diazocine is reported recently [37]. Synthesis, crystal structures and characterizations of three diclofenac-based copper complexes are reported by Alisir et al., [38]. Demir et al., reported the synthesis, crystal structure analysis of phenylpropanamide derivative experimentally and theoretically [39].

For various applications, the interaction between bio-molecules and metals has been researched in more depth utilizing various computational and experimental methodologies, especially surface enhanced Raman scattering [40,41]. Coinage metals, Au, Ag and Cu have a wide range of properties and are often utilized as catalysts in heterogeneous reactions. Bio-molecule interactions like FDC, with nanostructures are a popular issue in biological applications [42].

Computational chemistry has established itself as a reliable ally in the study of organic and biological structures, notably in a variety of chemistry fields. Theoretical chemical simulations have become critical in illuminating the molecule's architectures, characteristics, processes, and reaction effectiveness [43]. The most frequent theoretical approaches utilized in the calculation of various molecular properties include, optimal architectures, vibrational frequencies, nonlinear optical effects, and natural bond orbitals [44]. A range of spectroscopic analyses were used to characterize FDC in this study. FDC was investigated using DFT and vibrational spectra. The investigation was subjected to docking in order to determine exact binding location of ligand on protein as well as the mechanism of binding.

2. Methods

Synthesizing procedure of FDC was reported earlier and the title compound was a gift sample from R.L. Fine Chemicals, Bangalore, India, [30] and spectra (Fig.S1 and S2) were by Perkin Elmer and Bruker RFS-27 spectrophotometers. All quantum chemical studies of FDC (Fig. 1) are completed by Gaussian 09 with wB97XD/6–311++G* [45,46]. The default setting was used for the convergence criteria regarding SCF and optimization procedure. The potential energy distribution (PED)

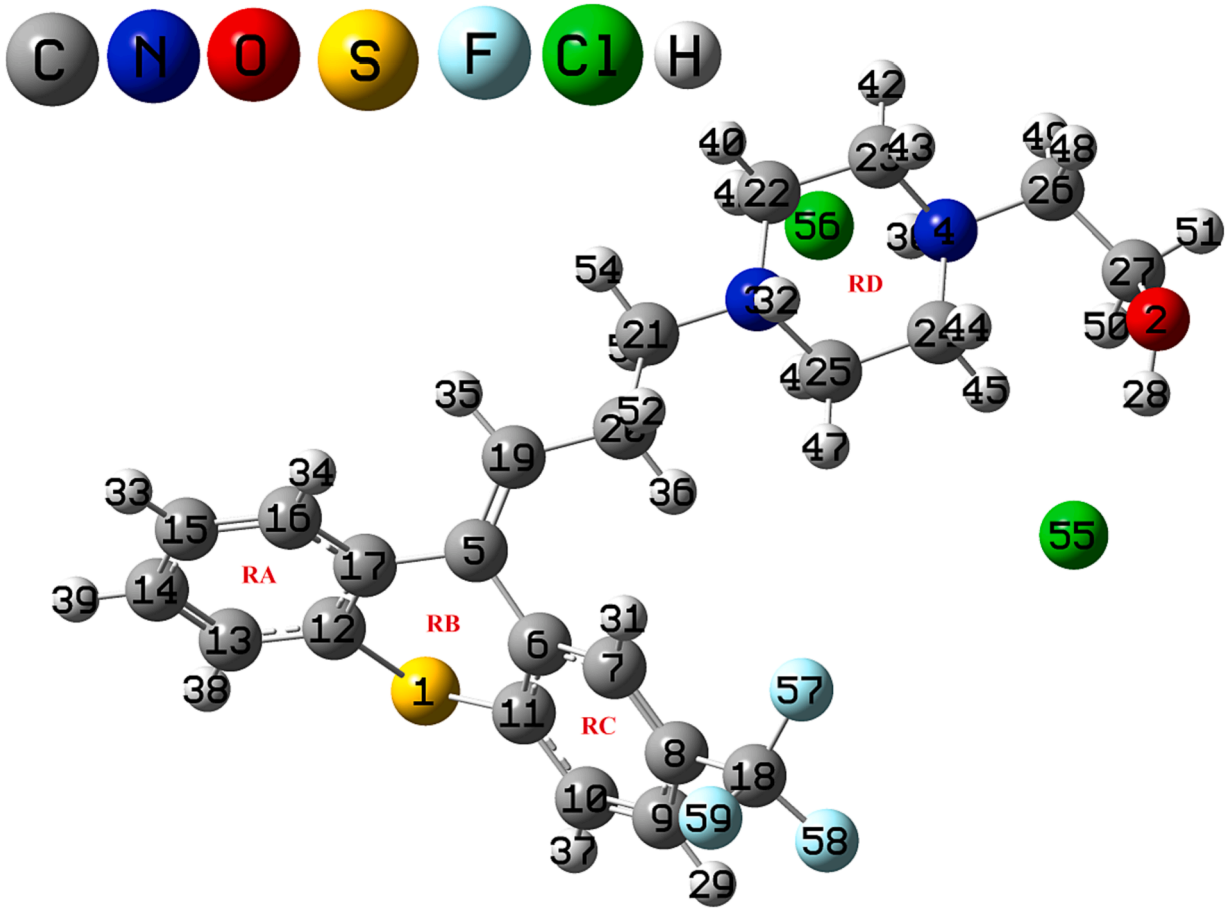

Fig. 1. Optimized geometry of FDC.

assignments are calculated using program GAR2PED [47]. A number of similar theoretical studies are reported recently [48–50]. Topological analysis was performed by Multiwfn [51–53]. Docking was done for FDC with PDB ID: 6YB7 [54,55]. The Desmond 2020.1 was used to run MD work [56]. Analysis was made to find root mean square deviation (RMSD), radius of gyration (Rg), root mean square fluctuation (RMSF), number H-bonds, and solvent accessible surface area (SASA) [57]. OPLS 2005 force field [58] has been used within NPT ensemble class. Simulation time was 10 ns, while solvent was treated with simple point charge (SPC) model [59]. MD simulations are also performed at temperatures, 300, 310, 320 to 330 K to find the influence of RMSD and RDF values in the presence of aqueous medium.

3. Results and discussion

3.1. Hirshfeld surface analysis

Electron density partitioning in the crystal system of any molecule can be analyzed using Hirshfeld Surface analysis which was mapped by the program, CrystalExplorer21 [60]. The 2D fingerprint plots and 3D Hirshfeld surfaces of FDC are in Fig. 2. There are enormous O_1-H_{1B}…Cl_1 (2.266 Å), N_1-H_{1A}…Cl_1 (2.102 Å), and C_9-H_{9A}…F_{3B} (2.655 Å) intermolecular hydrogen bonding were observed. It was reinforced by O-H…Cl (Sharp spikes), N-H…Cl and C-H…F which are 21.8%, 20.7%, and 12.6%, respectively. A greater contribution of about 30.2 % (H…H)

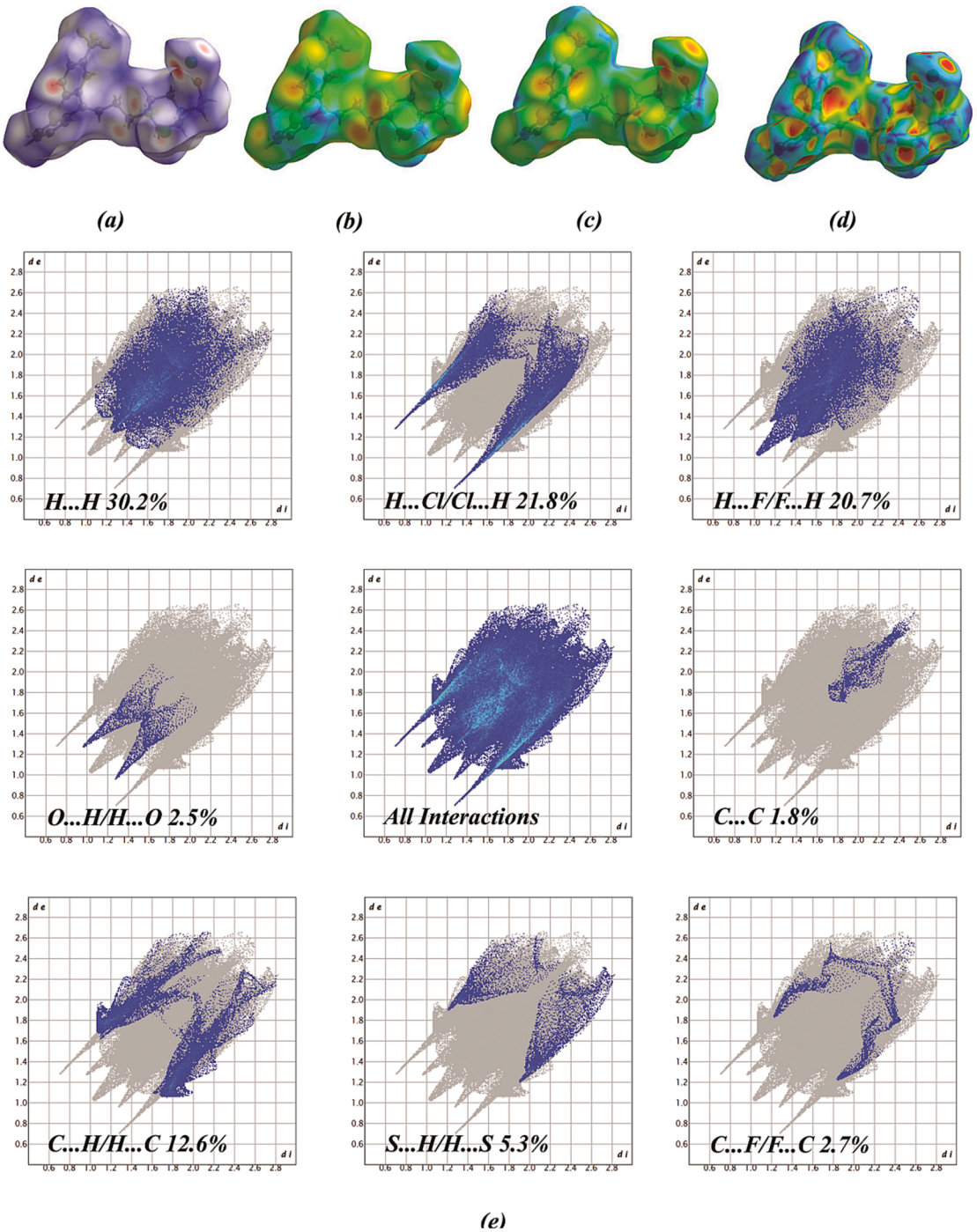

Fig. 2. Hirshfeld surface plots of FDC mapped with three-dimensional (a) dnorm, (b) di, (c) de, (d) Shape index and (e) two dimensional fingerprint contacts with its percentage contribution.

[61,62] in the overall 2D fingerprint plots which was due to active participation of hydrogen atoms. The stability of the system was further ascertained by Cl_1 atom which was bifurcated with N_1-H_{1A} and O_1-H_{1B} groups. On the other hand, fluorine atom enables a bridge between two adjacent aromatic systems. There are appreciable pi…pi interaction was observed with a % contribution of 1.8. A weak van der Waals interaction [63] between sulfur atom and hydrogen atoms of FDC was reflected by a percentage contribution of 5.3. From the 3D surface map, a weaker bow-tie pattern [64] expresses the possibility of lower centroid…centroid interaction that shows absence of π…π interactions in FDC.

A red spot was on the O–H and sulfur atom in d_{norm} which gives title compound has interaction zones. It is surprising that, fluorine atoms does not shows any red spots around it which may be due to the electron transfer may arise on C-H…F intermolecular bonding, that suppresses the electron density around fluorine [65].

3.2. Spectroscopic and electronic properties

The phenyl ring modes (table S1) are at: 3099–3072 (DFT) (υCH), 1609, 1580, 1463, 1442, 1036 (IR), 1609, 1575, 1465, 1266, 1035 (Raman), 1611–1035 cm^{-1} (DFT (υRA), 1221 (IR), 1222, 1122 (Raman), 1268–1122 cm^{-1} (DFT) (δCH) and at 868, 763 (IR), 970, 870 (Raman), 973–760 cm^{-1} (DFT) (γCH) for ring RA; 3115 (Raman), 3113–3090 (DFT) (υCH), 1628 (IR), 1630, 1588, 1055 (Raman), 1626–1053 cm^{-1} (DFT) (υRB), 1166, 1140 (IR), 1140 (Raman), 1252–1138 cm^{-1} (DFT) (δCH) and at 962, 911, 831 (IR), 910 (Raman), 960–830 cm^{-1} (DFT) (γCH) for ring RB [66,67].

The piperazine stretching modes, ring RD. are at 1125, 1072, 1025 (IR) and 1125, 1071, 1062, 1045, 1028, 920 cm^{-1} (DFT). The CH2 modes are at: 3068, 2995 (Raman), 3071–2924 cm^{-1} (DFT) (υCH2); 1421, 1393, 1358, 1325, 1261, 1006, 798 (IR), 1421, 1361, 1330, 1004 (Raman), 1458–803 cm^{-1} (DFT) (δCH2). The bands at 1358 and 1006 cm^{-1} in IR are characteristic vibrations of δCH2. Further CH2 of FDC are at: 3050, 2976, 2958, 2916 (IR), 2961, 2905 (Raman), 3044–2903 cm^{-1} (DFT) (υCH2); 1370, 1300, 1232 (IR), 1450, 1305, 1295, 1279, 1234, 1122 (Raman), 1475–893 cm^{-1} (DFT) (δCH2) [22,66].

Other important functional group modes are: υNH – 3334 (DFT), 3427 (IR), 3443 cm^{-1} (Raman); υOH – 3234 (DFT), 3306 (IR), 3385 cm^{-1} (Raman); υC = C – 1674 (DFT), 1660 (IR), 1675 cm^{-1} (Raman); υNH…Cl – 2366 (DFT), 2428 (IR), 2335 cm^{-1} (Raman); υCS – 700, 649 (DFT), 652 (IR), 653 cm^{-1} (Raman); υCF – 1313, 1176, 1133 (DFT), 1312 cm^{-1} (IR); υCO – 1095 (DFT), 1091 cm^{-1} (Raman). These results are in agreement with the reported literature [68–70]. The other deformation modes are also identified [66,71–73].

HOMO-LUMO analysis is used to identify the kinetic stability of any molecule by assessing the chemical reactivity through charge transfer process [74]. The electron cloud movement in FMOs is shown by red

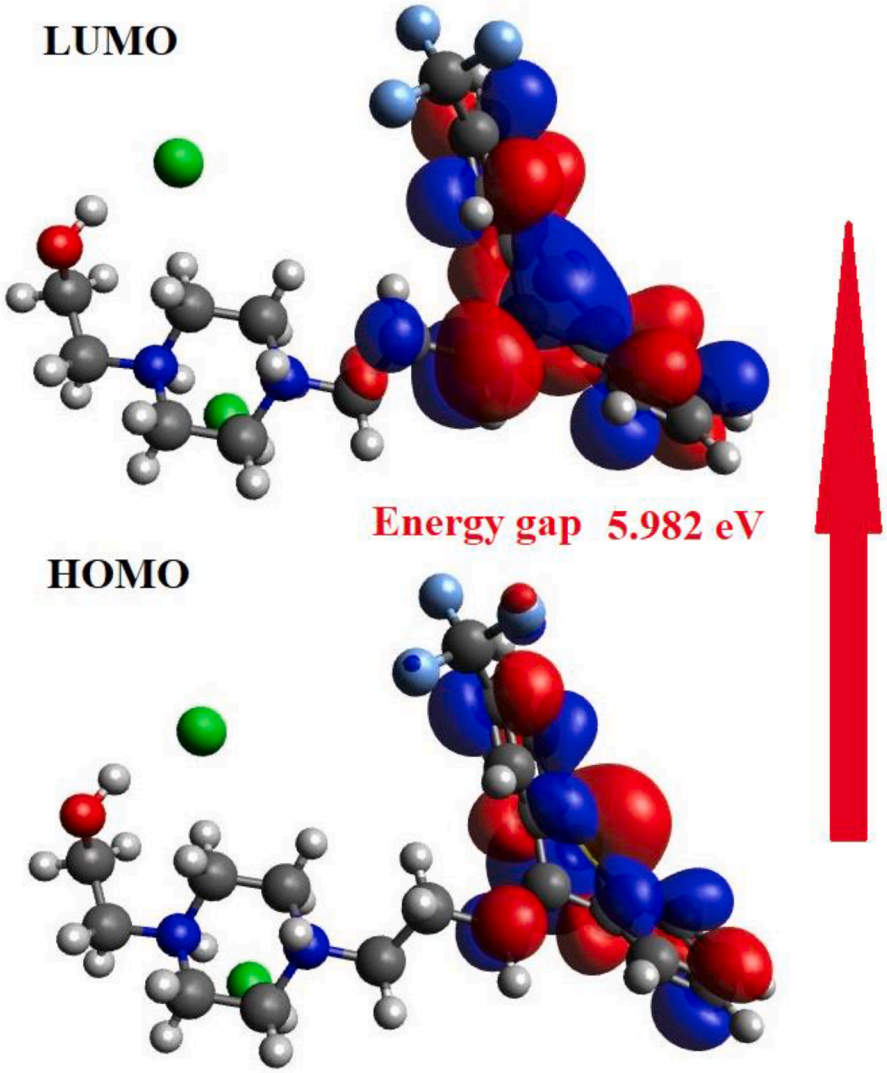

Fig. 3. HOMO-LUMO plots of FDC.

(positive) and blue (negative) (Fig. 3) [75–78]. Various electrophilic, nucleophilic and neutral sites of any molecular system can be easily analysed using molecular electrostatic potential analysis (MEP) through an electron mapping process which is used in various applications [79,80]. The negative and positive MEP corresponds to nucleophilic and electrophilic sites given by red and blue shades. Fig.S3 shows positive potential on C18, C19, C20, C21, N1 and N2 atoms [81]. Chlorine atoms Cl1 and Cl2 reveal a strong red colour that supports the electron rich centre [82]. It was clearly observed that, electrons were resonated on the aromatic ring systems of FDC without any interference with aliphatic moiety of both HOMO and in LUMO. It is due to the fluorine atom participated an enormous intermolecular hydrogen bonding with adjacent C–H (pi) system which was discussed in XRD, and Hirshfeld surface analysis elsewhere in this paper. The strong NBO interactions (table S2) are F58 → C18-F59, S1 → C10-C11, F57 → C18-C58, Cl55 → O2-N27 with energies 66.41, 14.07, 14.06, 22.39 kcal/mol [83]. For FDC, nearly 100% p-character is observed in n_2F_{57}, n_3F_{59}, n_2O_2, n_3Cl_{55}, n_2Cl_{56}, n_3F_{57}, n_2F_{58}, n_3F_{58}, and n_2F_{59} [84].

3.3. Topological and AIM analysis

The electron localization function (ELF) [85,86] characterizes the quantitative and qualitative ideas of electron density (ED) distribution by identifying molecular regions with maximal probability of finding the electron. Accordingly, the core and valence ELF attractors can be specified, and the synaptic order of valence basins indicates bonding and nonbonding electron density framework in a molecule. FDC's electronic structure (Fig.S4) is identified by two V(O) and V'(O) basins, with the population of 2.52 and 2.60, series of monosynaptic V(F) basins at the three fluorine atoms, series of monosynaptic V(Cl) basins at the two chlorine atoms, two V(S1) and V'(S1) integrating 4.22 e, two V(S1′,C2′) and V(S1′,C6′) basins of population of 2.82 and 1.74 e, two disynaptic V(N1,H) and V(N4,H) basins with 2.04 and 0.49 e, two V(C4′,C9) and V(C8,C9) with population of 3.67 e and 1.70 e, three disynaptic V(N1,C7), V(N1,C6) and V(N1,C2) basins with population of 1.67, 1.76 and 1.64 e, three V(N4,C10), V(N1,C5) and V(N1,C3) basins with population of 1.80, 2.13 and 2.14 e and one disynaptic V(C11,O) basin with the population of 2.13 e. The monosynaptic basins are associated with the nonbonding ED on oxygen, fluorine, chlorine and sulphur atoms shown as red localization domains in Fig. 4. The C4′-C9 bonding region integrating 3.67 e indicates the under populated C4-C9 olefinic double bond, owing to the delocalization across the thiopyran ring, revealed from total integrating with 2.82 and 1.74 with S1′-C2′ and S1′,C6′ bonding regions. The N4-H bonding region is highly depopulated compared to the N1-H owing to hydroxyethyl substitution in the former. The ELF shows under populated N-C single bonds of ring A owing to the strong electron withdrawing effect of N1 and N4 nitrogen atoms [87].

Bader and co-workers [88,89] proposed the QTAIM to characterize atomic interactions in a molecule. The computed bond and ring critical points (BCPs and RCPs) for FDC are shown in Fig. 5. The RCPs 67 and 119 associated with the phenyl rings C and D adjacent to the thiopyran ring show ED of 0.022 e with the positive LED 0.142, indicative of NCIs [90], which are represented as strongly repulsive ones (red regions) in the NCI isosurface (Fig. 5). RCPs 88 and 96 are with thiopyran and piperazine rings with ED of 0.018 and 0.022 and the Laplacian of ED 0.093 and 0.117 characteristic of NCIs. The NCI isosurface gives strongly attractive non-covalent interactions (blue regions) of the chlorine atoms and the adjacent hydrogen atoms, with the corresponding BCPs 66, 76, 81, 122 and 128 showing total ED of 0.010–0.053 e, the LED 0.033–0.095 and the LOL values of 0.157–0.367 e, suggestive of the hydrogen bond. Interestingly, RCP 125 is present at the vicinity of Cl and OH with ED of 0.010, Laplacian of ED 0.056 and LOL 0.101, while another RCP 72 at the vicinity of the second chlorine with ED of 0.011, Laplacian of ED 0.048 and LOL 0.130 (Fig. 5), which further reinforce the NCIs associated with the chlorine atoms. BCP 120 with the bond path connecting oxygen and piperazine carbon shows ED of 0.014, Laplacian of ED 0.065 and LOL 0.137. Finally, RCP 118 with ED of 0.013, Laplacian of ED 0.066 and LOL 0.127 is observed within the piperazine-hydroxymethyl-chlorine framework.

The reactive regions can be characterized using the MEP study. For FDC, MEP map is in Fig. 6, together with the ESP values at the surface maxima and surface minima. FDC shows presence of 13and 17 surface minima and maxima (magenta and cyan colour). The surface maxima with ESP value of + 93.70 and + 38.65 are over around the N1 nitrogen, while the surface minima with ESP of −74.35, −56.70 and −54.70 are around the chlorine atoms. The surface maxima with ESP value of + 14.49 is localized on N4 nitrogen. The MEP surface map also shows the presence of surface maxima with positive ESP of + 29.42 and + 29.70 kcal mol^{-1} along with three surface minima of negative ESP, −0.40, −4.96 and −6.89 kcal mol^{-1} at the vicinity of phenyl-thiopyran-phenyl framework. Two negative surface minima with ESP of −28.45 and −20.38 are around the fluorine atoms along with the surface maxima of + 12.28 kcal mol^{-1}.

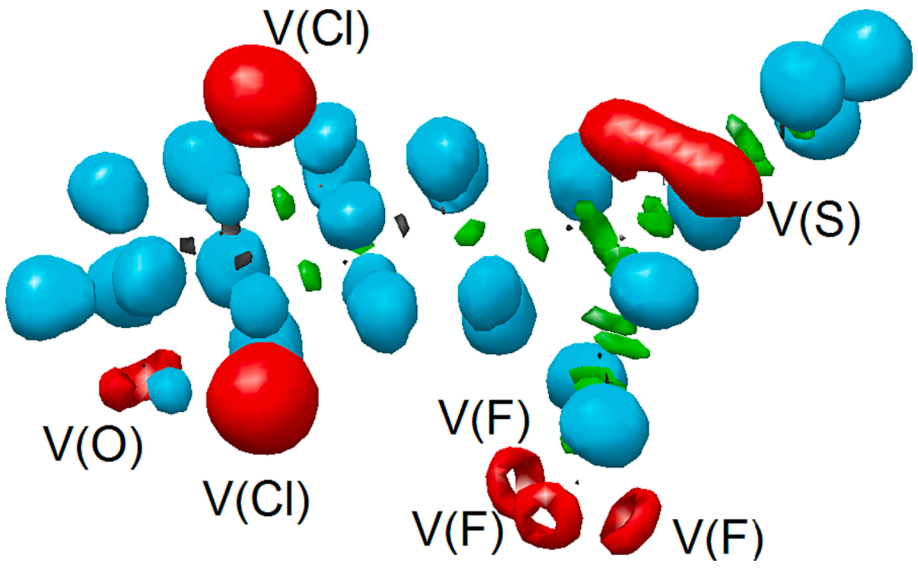

Fig. 4. ELF localization domains (Isovalue = 0.84) of FDC. The protonated basins are shown in blue, monosynaptic basins are marked in red, disynaptic basins are marked in green and the core basins are marked in red colour.

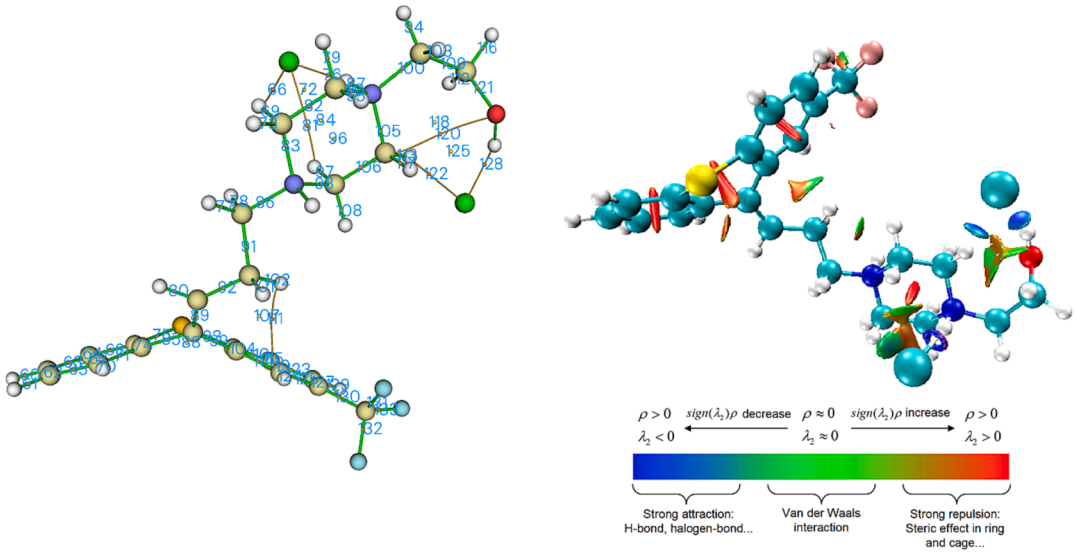

Fig. 5. BCPs (3,-1), RCPs (3,+1) and the bond paths along with the NCI isosurface of FDC.

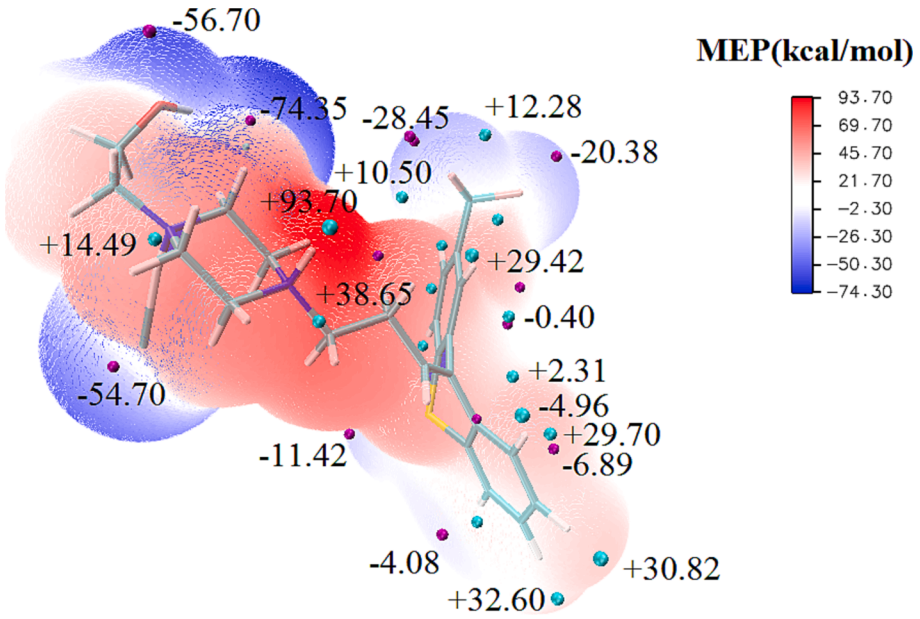

Fig. 6. Molecular Electrostatic Potential (MEP) isosurface with the electrostatic potential (ESP) in kcal/mol of the surface minima (magenta colour) and surface maxima (cyan colour).

3.4. Docking and MD simulations

Docking of FDC with the primary protease of the SARS-CoV (PDB ID: 6YB7) is shown in Fig.S5. Docking was performed by Autodock 4.2 [91]. The co-crystal was seen to be adequately accommodated within in the binding pocket of the surface view of the FDC with 6BY7 (Fig.S5). The dock score is determined using a tolerance of 0.5 Å RMSD and an area 616. The binding energy is −6.1 kcal/mol. Residue Met276 formed a conventional hydrogen bond with FDC (Fig.S5), while, the other residues produced weak interactions with FDC. The residues, TYR239, TYR237, LEU272, GLN273, THR199, LEU286, GLY275, LEU2711, LEU287, and ALA285 are interacting with FDC (Fig.S5).

MD simulation (100 ns) gives stable conformation while comparing the RMSD values of 6YB7 gives a deviation of 0.8 Å (Fig. 7(a)). During simulations, RMSD plots indicate convergence and stable conformations [92,93]. Therefore, it may be inferred that FDC's binding to 6YB7 formed a relatively stable complex as a result of FDCs increased affinity. Except for the residues that are conformed in to the loop region, which more flexible, the RMSF plots for 6BY7 protein show spikes of fluctuation. The residues show loess fluctuation (100 ns) on binding with FDC (Fig. 7b), indicating the stabile amino acid conformation. RMSF readings within the range that is acceptable. As a result, it is evident from RMSF plots that protein structures remain stable during FDC-6BY7 conformations [94]. The amount of H-bonds between 6BY7 and FDC suggests a substantial interaction and complex stability. Throughout the simulation of 100 ns, there were a considerable number of H-bonds between FDC bound with CoV-main protease (Fig. 7(c)). In order to help the complex formation into a stable complex, an average of 2 hydrogen bonds are seen for it in Fig. 7(c). Rg contributes the protein's complexation. The Rg of 6BY7 apo bound to FDC was reduced from 22.0 to 21.9 Å in our study (Fig. 7(d)).When the Rg is significantly reduced, 6BY7 is strongly oriented in a lignad-bound state [95]. Similar to Rg analysis, SASA in both ligand-bound and unbound state give the same behaviour. It is evident from Fig. 7(e) that SARS-CoV-2 major protease

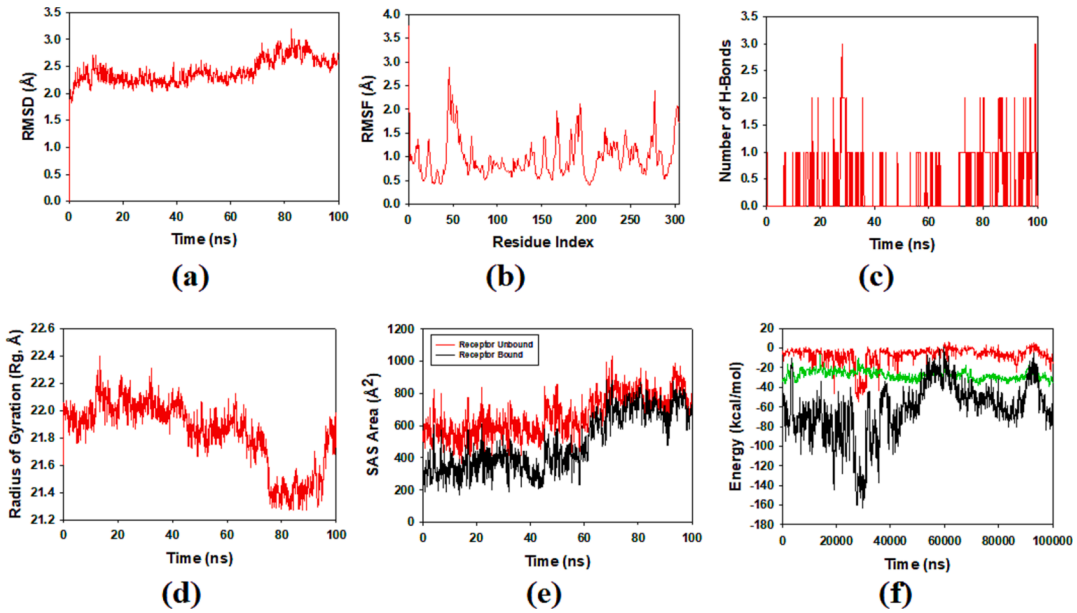

Fig. 7. MD simulation analysis of 100 ns trajectories of (a) Cα backbone of SARS-CoV-2 main protease + FDC (b) RMSF of Cα backbone of SARS-CoV-2 main protease + FDC (c) Formation of hydrogen bonds in SARS-CoV-2 main protease + FDC complex (d) Radius of gyration (Rg) of Cα backbone of SARS-CoV-2 main protease + FDC. (e) Solvent accessible surface area of SARS-CoV-2 main protease + FDC complex. (f) Energy plot of SARS-CoV-2 main protease + FDC complex.

had strong SASA when the FDC was not coupled to the receptor protein. When bound with FDC, the SASA value is lower than in the unbound condition [96]. The analysis of Rg shows that when FDC, the proteins are less flexible and more compact. The energy of the FDC-6BY7 complex in Fig. 7(f) is shown in energy plots. More negative values represent a more stable and compact structure. As can be seen in Fig. 7(f), the major protease of the SARS-CoV-2 virus achieved with an average energy −80 kcal/mol. Van der Waal's (vdW) and coulomb energies each contribute significantly to the achievement of the global minima (Fig. 7 (f)). Energy plots showed that both FDC could fit into the protein's binding cavity and help to stabilize the protein while also forming a compact complex.

We can explicitly account for the presence of water and impact of temperature in MD simulations. We can investigate a much more realistic liquid system in this way. More than 18,000 atoms make up the MD systems under consideration, which were housed in a cubic simulation box with side measuring 50 Å. This study's main goal was to run MD simulations at four different temperatures and see what happened to the interaction between the chosen ligands. By examining RDF calculated with regard to separation between the geometric centers of the ligand molecules, the interaction was examined. The human body need temperatures between 300 and 330 K, hence those values were chosen. The RDFs and RMSD plots are given in Figs. 8 and 9, which shows substantial interaction with the water molecules.

4. Conclusion

FDC was investigated using theoretically and experimentally and the investigation was subjected to docking to find binding location of ligand on the protein as well as the mechanism of binding. The stability of the

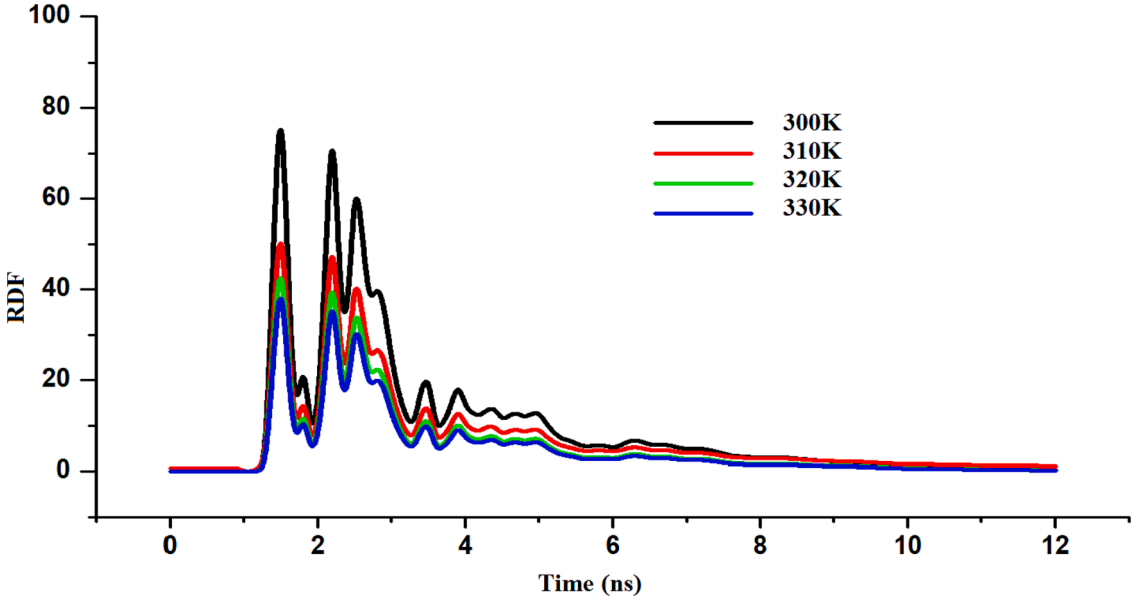

Fig. 8. RDF plots.

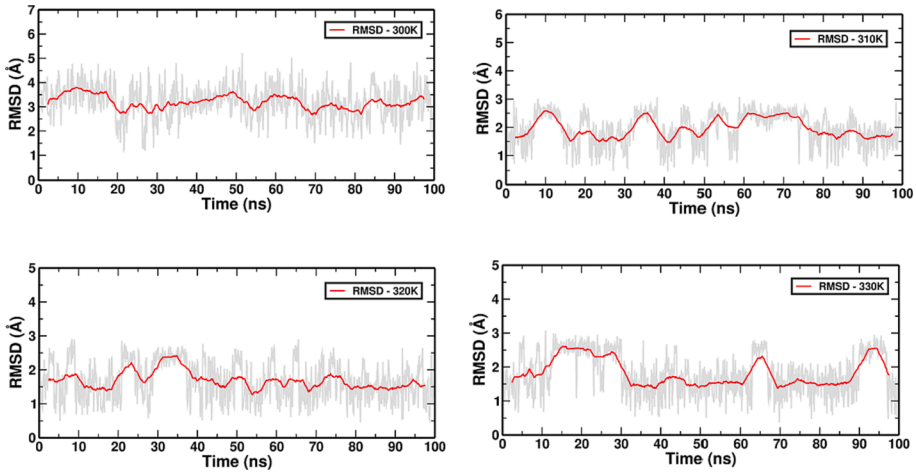

Fig. 9. RMSD plots at different temperatures.

system was ascertained by Cl_1 atom which was bifurcated with N_1-H_{1A} and O_1-H_{1B} groups and fluorine atom enables a bridge between two adjacent aromatic systems. The major protease of the SARS-CoV-2 virus achieved with an average energy −80 kcal/mol. The N4-H bonding region is highly depopulated compared to the N1-H owing to hydroxyethyl substitution in the former and the ELF shows under populated N-C single bonds of ring A owing to the strong electron withdrawing effect of N1 and N4 nitrogen atoms. The fluorine atom participated an enormous intermolecular hydrogen bonding with adjacent C–H (pi) system which was discussed in XRD, and Hirshfeld surface analysis. The NCI isosurface shows strongly attractive non-covalent interactions of the chlorine and adjacent hydrogen and LOL values suggest hydrogen bonds. 6BY7 bound to FDC displayed lowering of radius of gyration which shows highly compact orientation of the 6BY7-FDC bound state. RDF gives most substantial interactions with water molecules at different temperatures.

CRediT authorship contribution statement

Jamelah S.Al-Otaibi: Conceptualization, Methodology, Data curation, Software, Validation. **Y.Sheena Mary:** Conceptualization, Methodology, Data curation, Software, Validation. **Y.Shyma Mary:** Conceptualization, Methodology, Data curation, Software, Validation. **Nivedita Acharjee:** Conceptualization, Methodology, Data curation, Software, Validation. **Deepthi S. Rajendran Nair:** Conceptualization, Methodology, Data curation, Software, Validation. **H.S. Yathirajan:** Conceptualization, Methodology, Data curation, Software, Validation.

Declaration of Competing Interest

The authors declare that they have no known competing financial interests or personal relationships that could have appeared to influence the work reported in this paper.

Data availability

Data will be made available on request.

Acknowledgments

The authors express their gratitude to Princess Nourah bint Abdulrahman University Researchers Supporting Project number (PNURSP2023R13), Princess Nourah bint Abdulrahman University, Riyadh, Saudi Arabia

Appendix A. Supplementary material

Supplementary data to this article can be found online at https://doi.org/10.1016/j.molliq.2023.123177.

References

[1] A. Lecy, I. Agranat, Zinc-mediated reductive dimerizations of telluroxanthone and selenoxanthone, Tellurium-selenium selectivity, Tetrahedron Lett. 41 (2000) 6157–6160, https://doi.org/10.1016/S0040-4039(00)00997-7.
[2] M.A. Azuine, H. Tokuda, J. Takayasu, F. Enjyo, T. Mukainaka, T. Konoshima, H. Nishino, G.J. Kapadia, Cancer chemopreventive effect of phenothiazines and related tri-heterocyclic analogues in the 12-O-tetradecanoylphorbol-13-acetate promoted Epstein-barr virus early antigen activation and the mouse skin two stage carcinogenesis models, Pharmacol. Res. 49 (2004) 161–169, https://doi.org/10.1016/j.phrs.2003.07.014.
[3] P.M. LoRusso, B.J. Foster, A. Wozniak, L.K. Helibrun, J.I. McCormick, P.E. Ruble, M.A. Graham, J. Purvis, J. Rake, M. Drozd, G.F. Lockwood, T.H. Corbett, Phase I pharmacokinetic study of the novel antitumor agent SR233377, Clin. Cancer Res. 6 (2000) 3088–3094. https://clincancerres.aacrjournals.org/content/6/8/3088.
[4] N.S. Allen, D.J. Mallon, A.W. Timms, W.A. Green, F. Catalina, T. Corrales, S. Navaratnam, B.J. Parsons, Photochemistry and photocuring activity of novel 1-halogeno-4-propoxythioxanthones, J. Chem. Soc. Faraday Trans. 90 (1994) 83–92, https://doi.org/10.1039/FT9949000083.
[5] M. G. Neuman, M. H. Gehlen, M. V. Encinas, N. S. Allen T. Corrales, C. Peinado, F. Catalina, Photophysics and photoreactivity of substituted thioxanthones, J. Chem. Soc. Faraday Trans. 93 (1997) 1517-1520. https://doi.org/10.1039/A607264J.
[6] B. Dogan, S.A. Ozkan, B. Uslu, Electrochemical characterization of flupenthixol and rapid determination of the drug in human serum and pharmaceuticals by voltammetry, Anal. Lett. 38 (2005) 641–656, https://doi.org/10.1081/AL-200050312.
[7] H. Verdoux, M. Tournier, B. Begaud, Antipsychotic prescribing trends: a review of pharmaco-epidemiological studies, Acta Psychiatr. Scand. 121 (2010) 4–10, https://doi.org/10.1111/j.1600-0447.2009.01425.x.
[8] M.A. Schreiber, S.C. Armstrong, J.D. Markman, Psychotropic medication monitoring: a review, Prim. Care Companion CNS Disord. 21 (2019) 18r02324, https://doi.org/10.4088/PCC.18r02324.
[9] B. Varga, A. Csonka, A. Csonka, J. Molnar, L. Amarlal, G. Spengler, Possible biological and clinical applications of phenothiazines, Anticancer Res 37 (2017) 5983–5993. https://doi.org/10.21873/anticanres.12045.
[10] M. Tardy, M. Dold, R.R. Engel, S. Leucht, Trifluoperazine versus low potency girst generation antipsychotic drugs for schizophrenia, Cochrane Database Syst. Rev. 8 (2014) CD009396, https://doi.org/10.1002/14651858.CD009396.pub2.
[11] T. Parik, D. Goyal, J.R. Scarff, S. Lippmann, Antipsychotic drugs and safety concerns for breast feeding infants, South, Med. J. 107 (2014) 686–688. https://doi.org/10.14423/SMJ.0000000000000190.
[12] M. Retief, B. Chiliza, L. Phahladira, R. Emsley, L. Asmal, Prolactin, flupenthixol decanoate and first episode schizophrenia – clinical and laboratory correlates, Metab. Brain Dis. 34 (2019) 1679–1687, https://doi.org/10.1007/s11011-019-00474-5.
[13] K. Balasubramani, N. Sivarajasekar, S. Muthusaravanan, K. Ram, M. Naushad, T. Ahamad, G. Sharma, Efficient removal of antidepressant flupentixol using graphene oxide/cellulose nanogel composite: Particle swarm algorithm based artificial neural network modelling and optimization, J. Mol. Liquid. 319 (2020), 114371, https://doi.org/10.1016/j.molliq.2020.114371.
[14] A.S.A. Dena, S.A.A. Gaber, In vitro drug interaction of levocetirizine and diclofenac: Theoretical and spectroscopic studies, Spectrochim. Acta 181 (2017) 239–248, https://doi.org/10.1016/j.saa.2017.03.043.

[15] M.R. El-Zahry, B. Lendl, Structure elucidation and degradation kinetic study of ofloxacin using surface enhanced Raman spectroscopy, Spectrochim. Acta 193 (2018) 63–70, https://doi.org/10.1016/j.saa.2017.12.007.
[16] D. Raghav, S. Mahanty, K. Rathinasamy, Characterizing the interactions of the antipsychotic drug trifluoperazine with bovine serum albumin: probing the drug-protein and drug-drug interactions using multi-spectroscopic approaches, Spectrochim. Acta 226 (2020), 117584, https://doi.org/10.1016/j.saa.2019.117584.
[17] A.S. Beni, A.N. Chermahini, H. Sharghi, S.M. Monfared, MP2, DFT and ab initio calculations on thioxanthone, Spectrochim. Acta 82 (2011) 49–55, https://doi.org/10.1016/j.saa.2011.06.059.
[18] Y.S. Mary, C.Y. Panicker, T.S. Yamuna, M.S. Siddegowda, H.S. Yathirajan, A.A. Al-Saadi, C. Van Alsenoy, Theoretical investigations on the molecular structure, vibrational spectral, HOMO-LUMO and NBO analysis of 9-[3-(dimethylamino) propyl]-2-trifluoro-methyl-9H-thioxanthen-9-ol, Spectrochim. Acta 132 (2014) 491–501, https://doi.org/10.1016/j.saa.2014.05.016.
[19] V. Nagalakshmamma, M. Venkataswamy, P. Chiranjeevi, A.U. Maheswari, K. Tthyagaraju, C. Nagaraju, P.V. Chalapathi, Design, synthesis, anti-tobacco mosaic viral and molecule docking simulations of urea/thiourea derivatives of 2-(piperazine-1-yl)-pyrimidine and 1-(4-fluoro/4-chlorophenyl)-piperazine and 1-(4-chlorophenyl)-piperazine – A study, Bioorg. Chem. 102 (2020), 104084, https://doi.org/10.1016/j.bioorg.2020.104084.
[20] Y.S. Mary, C.Y. Panicker, H.T. Varghese, C. Van Alsenoy, M. Procházková, R. Ševčík, P. Pazdera, Acid-base properties, FT-IR, FT-Raman spectroscopy and computational study of 1-(pyrid-4-yl)piperazine, Spectrochim. Acta 121 (2014) 436–444, https://doi.org/10.1016/j.saa.2013.10.119.
[21] R. Renjith, Y.S. Mary, C.Y. Panicker, H.T. Varghese, M. Pakosińska-Parys, C. Van Alsenoy, T.K. Manojkumar, Spectroscopic (FT-IR, FT-Raman), first order hyperpolarizability, NBO analysis, HOMO and LUMO analysis of 1,7,8,9-tetra-chloro-10,10-dimethoxy-4-[3-(4-phenylpiperazin-1-yl)propyl]-4-azatricyclo [5.2.1.02,6]dec-8-ene-3,5-dione by density functional methods, Spectrochim. Acta 124 (2014) 500–513, https://doi.org/10.1016/j.saa.2014.01.045.
[22] R. Renjith, Y.S. Mary, C.Y. Panicker, H.T. Varghese, M. Pakozinska-Parys, C. Van Alsenoy, A.A. Al-Saadi, Spectroscopic (FT-IR, FT-Raman) investigations and quantum chemical calculations of 1,7,8,9-tetracholoro-10,10-dimethoxy-4-{3-[4-(3-methoxyphenyl)piperazin-1-yl]propyl}-4-azatricyclo[5.2.1.0.2,6]dec-8-ene-3,5-dione, Spectrochim, Acta 129 (2014) 438–450, https://doi.org/10.1016/j.saa.2014.03.077.
[23] D. Němečková, Y.S. Mary, C.Y. Panicker, H.T. Varghese, C. Van Alsenoy, M. Procházková, P. Pazdera, A.A. Al-Saadi, 1-Alkyl-1-methylpiperazine-1,4-diium Salts: Synthetic, Acid-Base, XRD-analytical, FT-IR, FT-Raman Spectral and Quantum Chemical Study, J. Mol. Struct. 1094 (2015) 210–236, https://doi.org/10.1016/j.molstruc.2015.03.051.
[24] K. S. Resmi, Y. S. Mary, H. T. Varghese, C. Y. Panicker, M. Pakosinska-Parys, C. Van Alsenoy, Spectral investigations, DFT computations and molecular docking studies of 1,7,8,9-tetrachloro-10,10-dimethoxy-4-{3-[4-(2-methylphenyl) piperazin-1-yl] propyl}-4-azatricyclo[5.2.1.02,6]dec-8-ene-3,5-dione, J. Mol. Struct. 1098 (2015) 130-145. https://doi.org/10.1016/j.molstruc.2015.05.047.
[25] A.T. Onawole, A.F. El-Ahmadi, Y.S. Mary, C.Y. Panicker, S. Armakovic, S. J. Armakovic, C. Van Alsenoy, A.A. Al-Saadi, Conformational, vibrational and DFT studies of a newly synthesized arylpiperazine-based drug and evaluation of its reactivity towards the human GABA receptor, J. Mol. Struct. 1147 (2017) 266–280, https://doi.org/10.1016/j.molstruc.2017.06.107.
[26] J.S. Al-Otaibi, A.H. Almuqrin, Y.S. Mary, Y.S. Mary, R. Thomas, Cocrystals of hydrochlorothiazide with picolinamide, tetramethylpyrazine and piperazine: quantum mechanical studies, docking and modeling of the photovoltaic efficiency for DSSC, J. Mol. Model. 26 (2020) 256, https://doi.org/10.1007/s00894-020-04528-9.
[27] A.Z. Omar, T.M. Mosa, S.K. El-sadany, E.A. Hamed, Novel piperazine based compounds as potential inhibitors for SARS-CoV-2 protease enzyme: Synthesis and molecular docking study, J. Mol. Struct. 1245 (2021), 131020, https://doi.org/10.1016/j.molstruc.2021.131020.
[28] O. Cakmar, S. Okten, D. Alimli, C.C. Ersanli, P. Taslimi, U.M. Kocyigit, Novel piperazine and morpholine substituted quinolines: selective synthesis through activation of 3,6,8-tribromoquinoline, characterisation and their some metabolic enzymes inhibition potentials, J. Mol. Struct. 1220 (2020), 128666, https://doi.org/10.1016/j.molstruc.2020.128666.
[29] H. Zhou, M.A. McGowan, K. Lipford, M. Christopher, X. Fradera, D. Witter, C. A. Lesburg, C. Li, J.L. Methot, J. Lampe, A. Achab, L. Shaffer, P. Goldenblatt, S. Shah, A. Bass, G. Schroeder, D. Chen, H. Zeng, M.A. Augustin, J.D. Katz, Discovery and optimization of heteroaryl piperazines as potent and selective PI3Kδ inhibitors, Bioorg. Med. Chem. Lett. 30 (2020), 126715, https://doi.org/10.1016/j.bmcl.2019.126715.
[30] M.S. Siddegowda, R.J. Butcher, M. Akkurt, H.S. Yathirajan, B. Narayana, 1-(2-Hydroxyethyl)-4-[3-(2-trifluoro-methyl-9H-thioxanthen-9-ylidene)-propyl] piperazine-1,4-diium dichloride: the dihydrochloride salt of flupentixol, Acta Cryst. E 67 (2011) o2079–o2080, https://doi.org/10.1107/S1600536811028182.
[31] I. Jomaa, N. Issaaoui, T. Roisnel, H. Marouni, Insight into non-covalent interactions in a tetrachlorocadmate salt with promising NLO properties: experimental and computational analysis, J. Mol. Stuct. 1242 (2021), 130730, https://doi.org/10.1016/j.molstruc.2021.130730.
[32] N. Issaoui, H. Ghalla, F. Bardak, M. Karabacak, N.A. Dlala, H.T. Flakus, B. Oujia, Combined experimental and theoretical studies on the molecular structures, spectroscopy, and inhibitor activity of 3-(2-thienyl)acrylic acid throughAIM, NBO, FT-IR, FT-Raman, UV and HOMO-LUMO analyses, and molecular docking, J. Mol. Struct. 1130 (2017) 659–668, https://doi.org/10.1016/j.molstruc.2016.11.019.
[33] C. Daghar, N. Issaoui, T. Roisnel, V. Dorcet, H. Marouani, Empirical and computational studies of newly synthesis cyclohexylammonium perchlorate, J. Mol. Struct. 1230 (2021), 129820, https://doi.org/10.1016/j.molstruc.2020.129820.
[34] M. Evecen, H. Tanak, F. Tinmaz, N. Dege, I. O. Ilhan, Experimental (XRD, IR and NMR) and theoretical investigations on 1-(2-nitrobenzoyl)3,5-bis(4-methoxyphenyl)-4.5-dihydro-1H-pyrazole, J. Mol Struct. 1126 (2016) 117-126, https://doi.org/10.1016/j.molstruc.2016.01.069.
[35] R. Ilmi, D. Zhang, J.D.L. Dutra, N. Dege, L. Zhou, W.-Y. Wong, P.R. Raithby, M. S. Khan, A tris β-diketonate europium (III) complex based OLED fabricated by thermal evaporation method displaying efficient bright red emission, Org. Electr. 96 (2021), 106216, https://doi.org/10.1016/j.orgel.2021.106216.
[36] P. Sen, G.Y. Atmaca, A. Erdogmus, S.D. Kanmazalp, N. Dege, S.Z. Yildiz, Peripherally tetra-benzimidazole units-substituted zinc(II) phthalocyanines: synthesis, characterization and investigation of photophysical and photochemical properties, J. Lumin. 194 (2018) 123–130, https://doi.org/10.1016/j.jlumin.2017.10.022.
[37] E. Aydemir, S. Kansiz, M.K. Gumus, N.Y. Gorobets, N. Dege, Crystal structure and Hirshfeld surface analysisof 7-ethoxy-5-methyl-2-(pyridine-3-yl)-11,12-dihydro-5,11-methano[1,2,4]triazolo[1,5-c]benzoxa-diazocine, Acta Cryst. E 74 (2018) 367–370, https://doi.org/10.1107/s2056989018002621.
[38] S. H. Alisir, N. Dege, R. Tapramz, Synthesis, crystal structures and characterizations of three new copper(II) complexes including anti-inflammatory diclofenac, Acta Cryst (2019) C75, https://doi.org/10.1107/s2053229619001827.
[39] S. Demir, A.O. Sarioglu, S. Guler, N. Dege, M. Sonmez, Synthesis, crystal structure analysis, spectral IR, NMR, UV-Vis investigations, NBO and NLO of 2-benzoyl-N-(4-chlorophenyl)-3-oxo-3-phenylpropanamide with the use of X-ray diffractions studies along with DFT calculations, J. Mol. Struct. 1118 (2016) 316–324, https://doi.org/10.1016/j.molstruc.2016.04.042.
[40] L. Fabris, S. Antonello, L. Armela, R. L. Donkers, F. Polo, C. Toniolo, F. Maran, Gold nanoclusters protected by conformationally constrained peptides, J. Am. Chem. Soc. 128 (2006) 326-336, https://doi.org/10.1021/ja056058110.1021/ja0560581.s001.
[41] Q. Yuan, Y. Wang, L. Zhao, R. Liu, F. Gao, L. Gao, X. Gao, Peptide protected gold clusters: chemical synthesis and biomedical applications, Nanoscale 8 (2016) 12095–12104, https://doi.org/10.1039/C6CR02750D.
[42] S. Pramanik, S. Chatterjee, A. Saha, P.S. Devi, G.S. Kumar, Unravelling the interaction of silver nanoparticles with mammalian and bacterial DNA, J. Phys. Chem. B 120 (2016) 5313–5324, https://doi.org/10.1021/acs.jpcb.6b01586.
[43] S.J. Armakovic, Y.S. Mary, Y.S. Mary, S. Pelemis, S. Armakovic, Optoelectronic properties of the newly designed 1,3,5-triazine derivatives with isatin, chalcone and acridone moieties, Comput. Theor. Chem. 1197 (2021), 113160, https://doi.org/10.1016/j.comptc.2021.113160.
[44] J.S. Al-Otaibi, A.H. Almuqrin, Y.S. Mary, Y.S. Mary, Comprehensive quantum mechanical studies on three bioactive anastrozole based triazole analogues and their SERS active graphene complex, J. Mol. Struct. 1217 (2020), 128388, https://doi.org/10.1016/j.molstruc.2020.128388.
[45] Gaussian 09, Revision B.01, M. J. Frisch, G. W. Trucks, H. B. Schlegel, G. E. Scuseria, M. A. Robb, J. R. Cheeseman, G. Scalmani, V. Barone, B. Mennucci, G. A. Petersson, H. Nakatsuji, M. Caricato, X. Li, H. P. Hratchian, A. F. Izmaylov, J. Bloino, G. Zheng, J. L. Sonnenberg, M. Hada, M. Ehara, K. Toyota, R. Fukuda, J. Hasegawa, M. Ishida, T. Nakajima, Y. Honda, O. Kitao, H. Nakai, T. Vreven, J. A. Montgomery, Jr., J. E. Peralta, F. Ogliaro, M. Bearpark, J. J. Heyd, E. Brothers, K. N. Kudin, V. N. Staroverov, T. Keith, R. Kobayashi, J. Normand, K. Raghavachari, A. Rendell, J. C. Burant, S. S. Iyengar, J. Tomasi, M. Cossi, N. Rega, J. M. Millam, M. Klene, J. E. Knox, J. B. Cross, V. Bakken, C. Adamo, J. Jaramillo, R. Gomperts, R. E. Stratmann, O. Yazyev, A. J. Austin, R. Cammi, C. Pomelli, J. W. Ochterski, R. L. Martin, K. Morokuma, V. G. Zakrzewski, G. A. Voth, P. Salvador, J. J. Dannenberg, S. Dapprich, A. D. Daniels, O. Farkas, J. B. Foresman, J. V. Ortiz, J. Cioslowski, D. J. Fox, Gaussian, Inc., Wallingford CT, 2010.
[46] R. Dennington, T. Keith, J. Millam, Gaussview, Version 5, Semichem Inc., Shawnee Mission, KS, 2009.
[47] J.M.L. Martin, C. Van Alsenoy, GAR2PED, a program to obtain a potential energy distribution from a Gaussian archive record, University of Antwerp, Belgium, 2007.
[48] A. Ramalingam, S. Sambandam, M. Medimagh, O. Al-Dossary, N. Issaoui, M. J. Wojcik, Study of a new piperidone as an anti-alzheimer agent: molecular docking, electronic and intermolecular interaction investigations by DFT method, J. King Saud Univ-Sci 33 (2021), 101632, https://doi.org/10.1016/j.jksus.2021.101632.
[49] C. Daghar, N. Issaoui, T. Roisnel, V. Dorcet, H. Marouani, Empirical and computational studies on newly synthesis cyclohexylammonium perchlorate, J. Mol. Struct. 1230 (2021), 129820, https://doi.org/10.1016/j.molstruc.2020.129820.
[50] M. Medimagh, N. Issaoui, S. Gatfaoui, O. Al-Dossary, A.S. Kazachenko, H. Marouani, M.J. Wojcik, Molecular modelling and biological activity analysis of new organic-inorgani hybrid: 2-(3,4-dihydroxyphenyl) ethanaminium nitrate, J. King Saud Univ-Sci. 33 (2021), 101616, https://doi.org/10.1016/j.jksus.2021.101616.
[51] T. Lu, F. Chen, Multiwfn: A multifunctional wavefunction analyzer, J. Comp. Chem. 33 (2012) 580–592, https://doi.org/10.1002/jcc.22885.
[52] W. Humphrey, A. Dalke, K. Schulten, VMD: Visual molecular dynamics, J. Mol. Graph. 14 (1996) 33, https://doi.org/10.1016/0263-7855(96)00018-5.
[53] E.F. Pettersen, T.D. Goddard, C.C. Huang, G.S. Couch, D.M. Greenblatt, C.C. Meng, T.E. Ferrin, UCSF Chimera–a visualization system for exploratory research and analysis, J. Comput. Chem. 25 (2004) 1605–1612, https://doi.org/10.1002/jcc.20084.

[54] https://www.rcsb.org/structure/6yb7.
[55] https://bioinfo3d.cs.tau.ac.il/PatchDock/php.php.
[56] W.L. Jorgensen, J. Chandrasekhar, J.D. Madura, R.W. Impey, M.L. Klein, Comparison of simple potential functions for simulating liquid water, J. Chem. Phys. 79 (1983) 926–935, https://doi.org/10.1063/1.445869.
[57] G.J. Martyna, D.J. Tobias, M.L. Klein, Constant pressure molecular dynamics algorithms, J. Chem. Phys. 101 (1994) 4177–4189, https://doi.org/10.1063/1.467468.
[58] J.L. Banks, H.S. Beard, Y. Cao, A.E. Cho, W. Damm, R. Farid, A.K. Felts, T. A. Halgren, D.T. Mainz, J.R. Maple, R. Murphy, D.M. Philipp, M.P. Repasky, L. Y. Zhang, B.J. Berne, R.A. Friesner, E. Gallicchio, R.M. Lew, Integrated modelling program, applied chemical theory (IMPACT), J. Comput. Chem. 26 (2005) 1752–1780, https://doi.org/10.1002/jcc.20292.
[59] H. J. Berendsen, J. P. Postma, W. F. van Gunsteren, J. Hermans, Interaction models for water in relation to protein hydration, in: Intermolecular forces, Springer, 1981, pp. 331-342, https://doi.org/10.1007/978-94-015-7658-1_21.
[60] J.J. McKinnon, M.A. Spackman, A.S. Mitchell, Novel tools for visualizing and exploring intermolecular interactions in molecular crystals, Acta Cryst. B 60 (2004) 627–668, https://doi.org/10.1107/s0108768104023000.
[61] M.A. Spackman, D. Jayatilaka, Hirshfeld surface analysis, CrstEngComm 11 (2009) 19–32, https://doi.org/10.1039/B818330A.
[62] S.K. Wolff, D.J. Grimwood, J.J. McKinnon, M.J. Turner, D. Jayatilaka, M. A. Spackman, CrystalExplorer -ver. 3.1, (University of Western Australia), 2012.
[63] A.D. Martin, J. Britton, T.L. Easun, A.J. Blake, W. Lewis, M. Schroder, Hirshfeld surface investigation of structure-directing interactions with dipicolinic acid derivatives, Cryst. Growth Des. 15 (2015) 1697–1706, https://doi.org/10.1021/cg5016934.
[64] J.B. Nanubolu, K. Ravikumar, Designing a new cocrystal of olanzapine drug and observation of concomitant polymorphism in a ternary cocrystal systems, CrstEngComm 19 (2017) 355–366, https://doi.org/10.1039/C6CE02227H.
[65] S. Balachandar, M. Sethuram, P. Muthuraja, M. Dhandapani, Bioactivity of a radical scavenger bis(pyrazolium p-toluenesulphonate) on ctDNA and certain microbes: a combined experimental and theoretical analysis, Toxicol. Res. 8 (2019) 421–431, https://doi.org/10.1039/C8TX00258D.
[66] N.P.G. Roeges, A guide to the complete interpretation of infrared spectra of organic structures, New York, John Wiley and Sons Inc., NY, 1994.
[67] J.S. Al-Otaibi, Y.S. Mary, S. Armakovic, R. Thomas, Hybrid and bioactive cocrystals of pyrazinamide with hydroxybenzoic acids: detailed study of structure, spectroscopic characteristics, other potential applications and noncovalent interactions using SAPT, J. Mol. Struct. 1202 (2020), 127316, https://doi.org/10.1016/j.molstruc.2019.127316.
[68] N. Rekik, N. Issaoui, H. Ghalla, B. Oujia, M.J. Wojcik, IR spectral density of H-bonds. Both intrinsic anharmonicity of the fast mode and the H-bond bridge. Part I: Anharmonic coupling parameter and temperature effects, J. Mol. Struct: THOECHEM. 821 (2007) 9–21, https://doi.org/10.1016/j.theochem.2007.06.016.
[69] N. Rekik, N. Issaoui, B. Oujia, M. J. Wojcik, Theoretical IR spectral density of H-bond in liquid phase: combined effects on anharmonicities, Fermi resonances, direct and indirect relaxations, J. Mol. Liq. 141 (2008) 104-109, https://doi.org/j.molliq.2007.10.009.
[70] A.S. Kazachenko, F. Akman, Y.N. Malyar, N. Issaoui, N.Y. Vasillieva, A. A. Karacharov, Synthesis optimization, DFT and physicochemical study of chitosan sulphates, J. Mol. Struct. 1245 (2021), 131083, https://doi.org/10.1016/j.molstruc.2021.131083.
[71] G. Socrates, Infrared characteristic group frequencies, John Wiley and Sons, New York, 1980.
[72] Y.S. Mary, C.Y. Panicker, C.N. Kavitha, H.S. Yathirajan, M.S. Siddegowda, S.M. A. Cruz, H.I.S. Nogueira, A.A. Al-Saadi, C. Van Alsenoy, J.A. War, Spectroscopic investigation (FT-IR, FT-Raman and SERS), vibrational assignments, HOMO-LUMO analysis and molecular docking study of opipramol, Spectrochim. Acta 137 (2015) 547–559, https://doi.org/10.1016/j.saa.2014.08.106.
[73] Y.S. Mary, C.Y. Panicker, B. Narayana, S. Samshuddin, B.K. Sarojini, C. Van Alsenoy, FT-IR, molecular structure, HOMO-LUMO, MEP, NBO analysis and first order hyperpolarizability of methyl 4,4''-difluoro-5'-methoxy-1,1':3'-1''-terphenyl-4'-carboxylate, Spectrochim. Acta 133 (2014) 480–488, https://doi.org/10.1016/j.saa.2014.06.031.
[74] K. Fulki, Role of frontier orbitals in chemical reactions, Science 218 (1982) 747–754, https://doi.org/10.1126/science.218.4574.747.
[75] J. Aihara, Reduced HOMO-LUMO gap as an index of kinetic stability for polycyclic aromatic hydrocarbons, Chem. A Eur. J. 103 (1999) 7487–7495, https://doi.org/10.1021/jp9900092i.
[76] A. Pirnau, V. Chis, O. Oniga, N. Leopold, L. Szabo, M. Baias, O. Cozar, Vibrational and DFT study of 5-(3-pyridyl-methylidene)-thiazolidine-2-thione-4-one, Vib. Spectrosc 48 (2008) 289–296, https://doi.org/10.1016/j.vibspec.2008.01.012.
[77] Y. Ruiz-Morales, HOMO–LUMO gap as an index of molecular size and structure for polycyclic aromatic hydrocarbons (PAHs) and asphaltenes: a theoretical study, Chem. A Eur. J. 106 (2002) 11283–11308, https://doi.org/10.1021/jp021152e.
[78] V.V. Aswathy, Y.S. Mary, P.J. Jojo, C.Y. Panicker, A. Bielenica, S. Armakovic, S. J. Armakovic, P. Brzozka, S. Krulowski, C. Van Alsenoy, Investigation of spectroscopic, reactive, transport and docking properties of 1-(3,4-dichlorophenyl)-3-[3-(trifluoromethyl)phenyl]thiourea (ANF-6): combined experimental and computational study, J. Mol. Struct. 1134 (2017) 668–680, https://doi.org/10.1016/j.molstruc.2017.01.016.
[79] P. Politzer, P.R. Laurence, K. Jayasuriya, Molecular electrostatic potentials: an effective tool for the elucidation of biochemical phenomena, Environ. Health Perspect. 61 (1985) 191–202, https://doi.org/10.1289/ehp.8561191.
[80] J. Lu, W.R. Kobertz, C. Deutsch, Mapping the electrostatic potential within the ribosomal exit tunnel, J. Mol. Biol. 371 (2007) 1378–1391, https://doi.org/10.1016/j.jmb.2007.06.038.
[81] T. Karthick, P. Tandon, Computational approaches to find the active binding sites of biological targets against busulfan, J. Mol. Model. 22 (2016) 142, https://doi.org/10.1007/s00894-016-3015-z.
[82] Y.S. Mary, Y.S. Mary, K.S. Resmi, V.S. Kumar, R. Thomas, B. Sureshkumar, Detailed quantum mechanical, molecular docking, QSAR prediction, photovoltaic light harvesting efficiency analysis of benzyl and its halogenated analogues, Heliyon 5 (2019) e02825.
[83] E. D. Glendening, A. E. Reed, J. E. Carpenter, F. Weinhold, NBO version 3.1, TCI, University of Wisconsin, Madison, 1998.
[84] A.E. Reed, L.A. Curtiss, F. Weinhold, Intermolecular interactions from a natural bond orbital, donor-acceptor, view point, Chem. Rev. 88 (1988) 899–926, https://doi.org/10.1021/cr00088a005.
[85] A.D. Becke, K.E. Edgecombe, A simple measure of electron localization in atomic and molecular systems, J. Chem. Phys. 92 (1990) 5397–5403, https://doi.org/10.1063/1.458517.
[86] B. Silvi, A. Savin, A., Classification of chemical bonds based on topological analysis of electron localization functions, Nature 371 (1994) 683–686. https://www.nature.com/articles/371683a0.
[87] J.S. Al-Otaibi, Y.S. Mary, Y.S. Mary, S. Soman, N. Acharjee, B. Narayana, Theoretical and experimental investigation of a pyrazole derivative-solvation effects, reactivity analysis and MD simulations, Chem. Phys. Lett. 793 (2022), 139469, https://doi.org/10.1016/j.cplett.2022.139469.
[88] R. F. W.Bader, In Atoms in Molecules: A quantum theory, Oxform, Clarendon Press, 1990.
[89] R.F.W. Bader, H. Essén, The characterization of atomic interactions, J. Chem. Phys. 80 (1984) 1943–1960, https://doi.org/10.1063/1.446956.
[90] J. C. -García, E. R. Johnson, S. Keinan, R. Chaudret, J. -P. Piquemal, D. N. Beratan, W. Yang, NCIPLOT: a program for plotting non-covalent interaction regions, J. Chem. Theory Comput. 7 (2011) 625-632. https://doi.org/10.1021/ct100641a.
[91] G.M. Morris, R. Huey, W. Lindstrom, M.F. Sanner, R.K. Belew, D.S. Goodsell, A. J. Olson, Autodock4 and Autodocktools4: automated docking with selective receptor flexibility, J. Comput. Chem. 16 (2009) 2785–2791, https://doi.org/10.1002/jcc.21256.
[92] A.C. Melvin, T.A. Annabelle, N.M. Marlon, A. Ghosh, In-silico evaluation of binding of phytochemicals from bayati (AnamirtacocculusLinn) to the glutathione-s-transferase of Asian Corn Borer (OstriniafurnacalisGuenée), J. Biomol. Struct. Dyn. 41 (2023) 2660–2666, https://doi.org/10.1080/07391102.2022.2036240.
[93] J.S. Al-Otaibi, Y.S. Mary, Y.S. Mary, R. Yadav, Structural and reactivity studies of pravadoline – An ionic liquid, with reference to its wavefunction-relative properties using DFT and MD simulations, J. Mol. Struct. 1245 (2021), 131074, https://doi.org/10.1016/j.molstruc.2021.131074.
[94] Y.S. Mary, Y.S. Mary, S. Armakovic, S.J. Armakovic, R. Yadav, I. Celik, R. Razavi, Investigation of reactive properties, adsorption on fullerene, DFT, Molecular dynamics simulation of an anthracene derivative targeting dihydrofolate reductase and human dUTPase, J. Biomol. Struct. Dyn. 40 (2022) 10952–10961, https://doi.org/10.1080/07391102.2021.1953602.
[95] G. Venkatesh, Y. Sixto-Lopez, P. Vennila, Y.S. Mary, J. Correa-Basurto, Y.S. Mary, A. Manikandan, An investigation on the molecular structure, interaction with metal clusters, anti-covid-19 ability of 2-deoxy-D-glucose: DFT calculations, MD and docking simulations, J. Mol. Struct. 1258 (2022), 132678, https://doi.org/10.1016/j.molstruc.2022.132678.
[96] L.H. Al-Wahaibi, M. Abdalla, Y.S. Mary, Y.S. Mary, R.A. Costa, M. Rana, A.A. El-Emam, H.M. Hassan, N.H. Al-Shaalan, Spectroscopic, solvation effects and MD simulation of an adamantane-carbohyrazide derivative, a potential antiviral agent, Polycycl. Aro. Compound. 43 (2023) 2056–2070, https://doi.org/10.1080/10406638.2022.2039233.